Liu *et al. Energy Mater.* **2025**, *5*, 500058
DOI: 10.20517/energymater.2024.175

Energy Materials

Article

Open Access

Check for updates

Joule heating to grain-boundary-rich RuP_2 for efficient electrocatalytic hydrogen evolution in a wide pH range

Tingting Liu[1,3,#], Chen Chen[1,#], Zonghua Pu[1,2,*], Xiaofeng Zhang[1], Qiufeng Huang[1], Abdullah M. Al-Enizi[2], Ayman Nafady[2], Zhangsen Chen[3], Shuhui Sun[3,*], Gaixia Zhang[4,*]

[1]Fujian Key Laboratory of Polymer Science, Fujian Provincial Key Laboratory of Advanced Materials Oriented Chemical Engineering, College of Chemistry & Materials Science, Fujian Normal University, Fuzhou, 350117, Fujian, China.
[2]Department of Chemistry, College of Science, King Saud University, Riyadh 11451, Saudi Arabia.
[3]Institut National de la Recherche Scientifique (INRS), Centre Énergie Matériaux Télécommunications, Varennes J3X 1P7, Canada.
[4]Department of Electrical Engineering, École de Technologie Supérieure (ÉTS), Montreal H3C 1K3, Canada.
[#]Authors contributed equally.

[*]**Correspondence to:** Prof. Zonghua Pu, College of Chemistry & Materials Science, Fujian Normal University, No. 18, Wulongjiangzhong Road, Shangjie Town, Minhou County, Fuzhou 350117, Fujian, China. E-mail: zonghua.pu@fjnu.edu.cn; Prof. Shuhui Sun, Institut National de la Recherche Scientifique (INRS), Centre Énergie Matériaux Télécommunications, 1650 Lionel-Boulet Blvd, Varennes J3X 1P7, Canada. E-mail: shuhui.sun@inrs.ca; Prof. Gaixia Zhang, Department of Electrical Engineering, École de Technologie Supérieure (ÉTS), 1100 Notre-Dame St W, Montreal H3C 1K3, Canada. E-mail: gaixia.zhang@etsmtl.ca

How to cite this article: Liu, T.; Chen, C.; Pu, Z.; Zhang, X.; Huang, Q.; Al-Enizi, A. M.; Nafady, A.; Chen, Z.; Sun, S.; Zhang, G. Joule heating to grain-boundary-rich RuP_2 for efficient electrocatalytic hydrogen evolution in a wide pH range. *Energy Mater.* **2025**, *5*, 500058. https://dx.doi.org/10.20517/energymater.2024.175

Received: 16 Sep 2024 **First Decision:** 14 Nov 2024 **Revised:** 12 Dec 2024 **Accepted:** 20 Dec 2024 **Published:** 26 Feb 2025

Academic Editor: Sining Yun **Copy Editor:** Ping Zhang **Production Editor:** Ping Zhang

Abstract

The production of storable hydrogen fuel through water splitting, powered by renewable energy sources such as solar photovoltaics, wind turbines, and hydropower systems, represents a promising path toward achieving sustainable energy solutions. Transition-metal phosphides (TMPs) have excellent physicochemical properties, making them the most promising electrocatalysts for hydrogen evolution reaction (HER). Traditionally, achieving good crystallinity in these TMPs typically requires prolonged (≥ 2 h) high-temperature pyrolysis, which is time-consuming and generally yields samples with large particle sizes, adversely affecting the catalytic activities. Herein, for the first time, we present a groundbreaking discovery in the synthesis of grain-boundary-rich RuP_2 nanoparticles within a very short time frame of nine seconds, using a fast Joule heating strategy (RuP_2 JH). Subsequent electrochemical tests reveal that the as-synthesized RuP_2 JH not only exhibits platinum-like HER activity, achieving overpotentials of 22 mV, 22 mV and 270 mV to reach a current density of 10 mA cm^{-2} in 0.5 M

H_2SO_4, 1.0 M KOH, and 0.1 M phosphate buffered solutions, respectively, but also exhibits exceptional long-term stability. Moreover, it exhibits a Faradaic efficiency exceeding 96%. This work significantly contributes to the expanding repertoire of TMPs synthesized via Joule heating by showcasing exceptional performance toward HER and other energy-related catalytic applications.

Keywords: Transition-metal phosphides, Joule heating, grain boundary engineering, water splitting, hydrogen evolution reaction

INTRODUCTION

The increasing global energy demand, along with the consequential climate changes and environmental issues, has prompted both science and industry to explore sustainable and environmentally friendly alternative sources of energy as a substitute for depletable fossil fuels. Due to its high calorific value, superior energy density, and complete absence of carbon emissions, hydrogen is widely recognized as an optimal energy carrier[1-3]. The production of green hydrogen via a water electrolyzer, facilitated by renewable energy sources such as solar, wind, and hydropower, represents a promising avenue toward achieving sustainable energy solutions. Platinum (Pt)-based compounds remain the most effective electrocatalysts for hydrogen evolution reaction (HER: $2H^+ + 2e^- \rightarrow H_2$)[4-6]. Nevertheless, the commercialization of Pt as an electrocatalyst for widespread H_2 production is hindered by its exorbitant cost and limited availability[7]. Therefore, it is crucial to identify cost-effective, high-performance, and durable alternative catalysts to efficiently catalyze the hydrogen evolution reaction (HER).

In the past decades, transition-metal phosphides (TMPs) have attracted considerable attention due to their outstanding physicochemical properties, including good conductivity and high catalytic activities[8-12]. However, developing Pt-group metal (PGM)-free TMPs that offer catalytic performance comparable to or exceeding that of Pt remains a significant challenge. Therefore, PGM-based TMPs are often considered the optimal choice. Among these, ruthenium (Ru) emerges as the most promising noble metal for this purpose. Recent studies have reported various Ru-based phosphides, such as RuP_2, RuP, and Ru_2P, exhibiting HER performance that is comparable to or even surpasses that of commercial Pt/C catalysts[13,14]. For example, Mu's group first demonstrated that N,P dual-doped carbon-encapsulated RuP_2 catalyst exhibits Pt-like activity towards HER under a wide pH range[15]. Additionally, Ru_2P/C was synthesized by Ishikawa *et al.* using a temperature-programmed reduction method with H_2 as the reductant[16]. Notably, most TMPs were synthesized through high temperature and/or high-pressure pyrolysis of the metal and phosphorus precursors over extended reaction times (≥ 2 h)[17-19]. In general, these conventional methods for preparing TMPs are not only energy-intensive, but also result in larger grain sizes and lower surface areas due to prolonged pyrolysis, leading to a decreased electrochemical performance[20-22]. Therefore, it is highly desirable to explore alternative synthetic approaches that enable the production of TMPs with smaller nanoparticle sizes and increased surface areas through lower pyrolysis temperatures or shorter pyrolysis durations.

Recently, due to its ultrafast heating process in milliseconds to ~3,000 °C, Joule heating has received widespread utilization in the synthesis of various nanomaterials with ultrafine nanostructures, such as materials-based single atoms, nanocrystals composed of transition metal carbide and intermetallic nanoparticles with a size distribution of approximately ~6 nm[23-26]. The primary advantage of Joule heating lies in its ability to achieve sintering in seconds, thereby preventing the occurrence of sintering and agglomeration of active components in prolonged heat treatment. Undoubtedly, this ensures rapid and effective dispersion of active atoms, facilitating precise regulation of particle size, and structure in the synthesized material. On the other hand, several studies have demonstrated the superior catalytic efficiency

of P-rich TMPs compared to their P-deficient counterparts in HER[10,27,28]. Furthermore, when it comes to noble metal-based catalysts, doping with phosphorus elements has been proven effective in reducing the reliance on noble metals while enhancing their catalytic activity. However, the synthesis of P-rich TMPs is challenging due to prolonged pyrolysis resulting in the decomposition of the P-rich TMPs to P-deficient TMPs[29].

Drawing inspiration from the aforementioned descriptions, this study demonstrates that Joule heating for just nine seconds enables the synthesis of grain-boundary-enriched, P-rich RuP_2 (RuP_2 JH). Remarkably, the obtained RuP_2 JH exhibits platinum-like HER activity with overpotentials of 22, 22 and 270 millivolts at a current density of 10 milliamperes per square centimeter in 0.5 M H_2SO_4, 1.0 M KOH and 0.1 M phosphoric acid buffer solution, respectively. These high HER activities not only surpass the majority of previously reported electrocatalysts based on precious-metal-based phosphides but also rival the activity of state-of-the-art commercial Pt/C materials. Therefore, this study presents a pioneering approach to fabricating TMPs in seconds by Joule heating, resulting in enhanced performance in HER and other energy conversion and storage devices.

EXPERIMENTAL

Chemicals

The reagents $(NH_4)_2RuCl_6$, red P, H_2SO_4, KOH, NaH_2PO_4, and Na_2HPO_4 were used without further purification as received. The Nafion (5 wt%) and commercial Pt/C catalyst (20 wt%) were obtained from Sigma-Aldrich. High-purity H_2O was supplied by a Millipore system.

Joule heating synthesis of RuP_2

Typically, 40 mg of $(NH_4)_2RuCl_6$ and 17.3 mg of red P were finely ground under anhydrous and oxygen-free conditions. Subsequently, the precursor mixture underwent Joule heating (current ~80 A, potential ~36 V, thermal shock time ~9 s) in an Ar flow. After cooling, the resulting black product was subjected to three washes with deionized water to eliminate by-products. The final product was subjected to vacuum drying at 60 °C in a specialized oven.

The preparation of the catalyst ink

The electrocatalyst ink solution was prepared by mixing 4.0 mg RuP_2 catalyst and 1.0 mg carbon black with 300 μL ethanol, 100 μL water, and 10 μL Nafion (5 wt%). Subsequently, the mixture was subjected to sonication for a duration of 30 min to ensure homogeneous mixing. The working electrode was obtained by depositing 7.0 μL of the catalyst ink onto a 3 mm diameter glassy carbon electrode with a loading weight of 0.97 mg_{RuP_2} cm^{-2}. As a benchmark catalyst in this study, commercial 20 wt% Pt/C (loading weight: 0.71 mg cm^{-2}) was employed.

Materials characterization

Transmission electron microscopy (TEM) images were collected using a JEOL-2100F field-emission gun transmission electron microscope operating at 200 kV. X-ray powder diffraction (XRD) patterns of the as-obtained catalysts were collected using a Rigaku D/MAX-RB diffractometer equipped with monochromatized Cu-Kα radiation at 50 mA and 40 kV. The X-ray photoelectron spectroscopic (XPS) data was acquired using a VG Multi-lab 2000 instrument.

Electrochemical testing

The electrochemical performance was assessed using a standard three-electrode configuration at ambient temperature. All electrochemical measurements were conducted on an electrochemical workstation (CHI 750E, CH Instrument, Shanghai Chenhua, China). The electrochemical tests were performed in 0.5 M

sulfuric acid, 0.1 M phosphate-buffered saline (PBS), and 1.0 M KOH solutions. The reference electrode employed in this study was a saturated calomel electrode (SCE), while a graphite bar was utilized as the counter electrode. The SCE was calibrated against the reversible hydrogen electrode (RHE) in all measurements. The *iR*-corrected potential was determined by incorporating the internal resistance correction obtained from electrochemical impedance spectroscopy (EIS), as given in:

$$E_{corrected} = E_{test} - iR \times 100\% \quad (1)$$

where E_{test}, R, and i represent the initial potential, internal resistance and corresponding current, respectively. $E_{corrected}$ refers to the potential adjusted for the effects of *iR*.

The Faradic efficiency (FE) is determined by experimentally measuring the amount of H_2 produced and comparing it to the theoretically expected yield, quantifying the extent of agreement between experimental and theoretical values. A water drainage technique was employed to collect the H_2. The electrode was subjected to a constant potential, while the concurrent measurement of evolved gas volume was conducted. The moles of H_2 were subsequently determined using gas laws, followed by the calculation of the theoretically anticipated quantity of hydrogen based on Faraday's law. This law states that 96485 C passing through the system causes 1 equivalent of reaction.

RESULTS AND DISCUSSION

The detailed synthesis process for the RuP_2 nanoparticles through the Joule heating method is illustrated in Figure 1A. Initially, a homogeneous mixture of ammonium chlororuthenite (IV) and red P was prepared. Next, the obtained precursor mixture underwent Joule heating under an argon flow. After cooling and rinsing with deionized water to eliminate the by-product chloride ions, *etc.*, the final product of RuP_2 JH was obtained.

The morphology of RuP_2 JH is initially characterized using high-angle annular dark-field scanning TEM (HAADF-STEM). The low-magnification TEM image in Figure 1B reveals the presence of numerous nanoparticles within RuP_2 JH. The high-magnification TEM image further reveals that the RuP_2 JH exhibits a particle diameter ranging from 15 nm to 60 nm, as shown in Figure 1C and Supplementary Figure 1. This suggests that the resulting material displays a relatively good uniformity. However, further control experiments should be conducted in future research to improve the homogeneity of the nanoparticles. In contrast, the bulk RuP_2 obtained through conventional pyrolysis at 800 °C for 2 h under an inert atmosphere shows a particle size exceeding 200 nm [Supplementary Figure 2]. Therefore, the small nanoparticle size of RuP_2 obtained can be attributed to the rapid JH method, which effectively prevents sintering and agglomeration typically induced by prolonged heat treatment. Consequently, it guarantees prompt and efficient dispersion of active atoms, while simultaneously controlling the micro-morphology, composition, and structure of synthetic materials. Crucially, the presence of grain boundaries is pervasive within the RuP_2 JH nanoparticles [Figure 1D], which can be attributed to the ultrafast heating and cooling process during sample processing. Additionally, the high-resolution TEM (HRTEM) image in Figure 1E reveals a well-defined lattice fringe measuring 0.386 nm, which closely corresponds to the observed diffraction pattern associated with the (110) crystal plane of orthorhombic phase RuP_2[30]. The energy dispersive spectroscopy (EDS) analysis reveals the presence of both P and Ru signals in the RuP_2 JH samples [Supplementary Figure 3]. Moreover, the RuP_2 JH nanoparticles exhibit a uniform distribution of both P and Ru elements, as evidenced by HAADF-STEM and EDS elemental mapping images [Figure 1F-I].

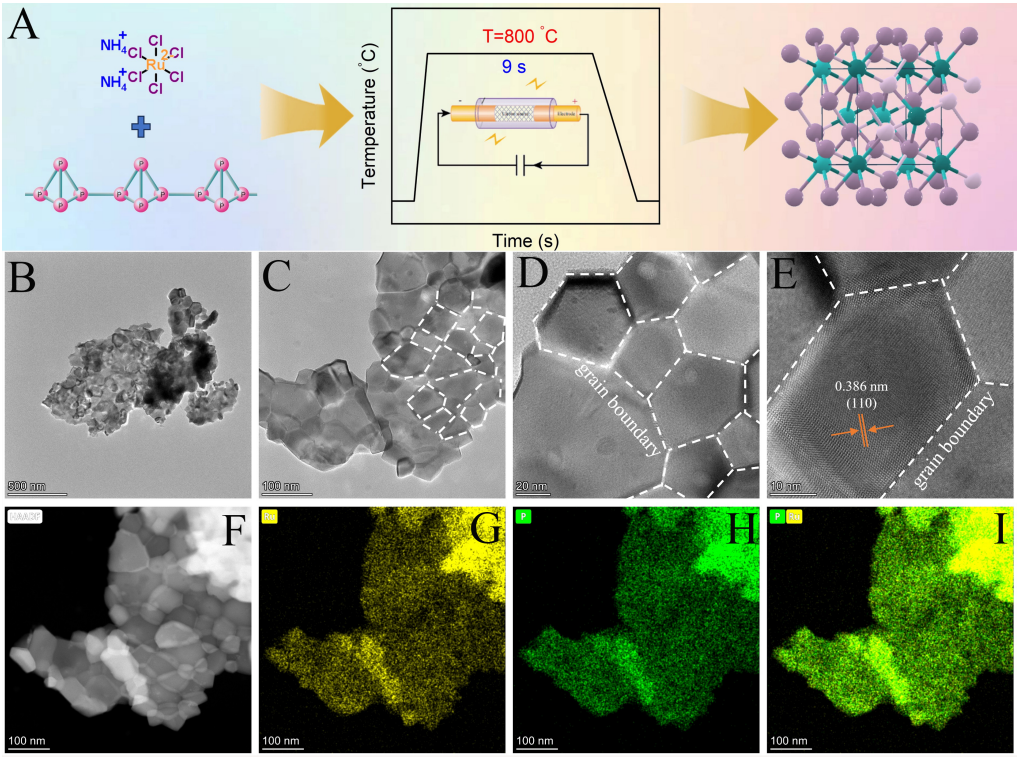

Figure 1. (A) Schematic diagram for the preparation of RuP_2 nanoparticles by JH method; (B-D) Low- and high-magnification TEM images of RuP_2 JH; (E) HRTEM, and (F-I) HAADF images and corresponding EDS elemental mapping of Ru and P of RuP_2 JH. TEM: Transmission electron microscopy; HRTEM: high-resolution TEM; HAADF: high-angle annular dark-field; EDS: energy dispersive spectroscopy.

The powder XRD was used to investigate the crystallographic structure of RuP_2 JH. As illustrated in Figure 2A, the obtained sample exhibited a well-matched powder XRD pattern with the orthorhombic RuP_2 phase as indicated by the standard PDF card (PDF No. 34-0333). The space group was determined as Pnnm(58) with cell parameters a_0 = 5.12 Å, b_0 = 5.89 Å, c_0 = 2.87 Å; Supplementary Figure 4 provides a visual representation[31]. Additionally, XPS was employed to investigate the intricate elemental composition and surface chemical state of RuP_2 JH. The obtained results reveal that the surface of RuP_2 JH is predominantly composed of Ru, P, C, and O [Supplementary Figure 5]. The presence of elemental C and O can be attributed to the absorbed CO_2, H_2O, and O_2, or to slight surface oxidation of RuP_2 JH due to potential exposure to air. The XPS spectrum of the Ru 3d and C 1s regions [Figure 2B] reveals peaks at binding energies (BEs) of 284.5 eV and 280.4 eV, which correspond to the Ru $3d_{3/2}$ and Ru $3d_{5/2}$ states of RuP_2 JH, respectively. Concerning the Ru 3p spectrum, the peaks detected at BEs of 461.9 eV and 484.3 eV can be ascribed to the Ru $3p_{3/2}$ and Ru $3p_{1/2}$ states [Figure 2C], respectively. It is noteworthy that the peak of Ru $3p_{3/2}$ is blue-shifted by 0.4 eV from the metal Ru (461.5 eV)[32]. The blue shift primarily arises from the bonding structures involving Ru-P. Furthermore, Figure 2D illustrates the P 2p spectrum, which exhibits three distinct subpeaks at 133.7 eV, 130.3 eV and 129.6 eV, respectively. The peaks observed at BEs of 130.3 eV and 129.6 eV can be attributed to the presence of the Ru-P bond, while the peak detected at BE of 133.7 eV suggests the existence of oxidized phosphorus species (PO_4^{3-}). It is noteworthy that the P $2p_{3/2}$ peaks in RuP_2 JH exhibit a negative shift compared to elemental phosphorus (130.2 eV)[33]. These observations suggest the presence of a partial negative charge (δ^-) on P and a partial positive charge (δ^+) on Ru in RuP_2 JH, indicating a weak electron transfer from Ru to P. The negatively charged P atom tends to attract a positively charged proton, similar to a base, thereby modulating the ability of active sites H atoms to attach and detach

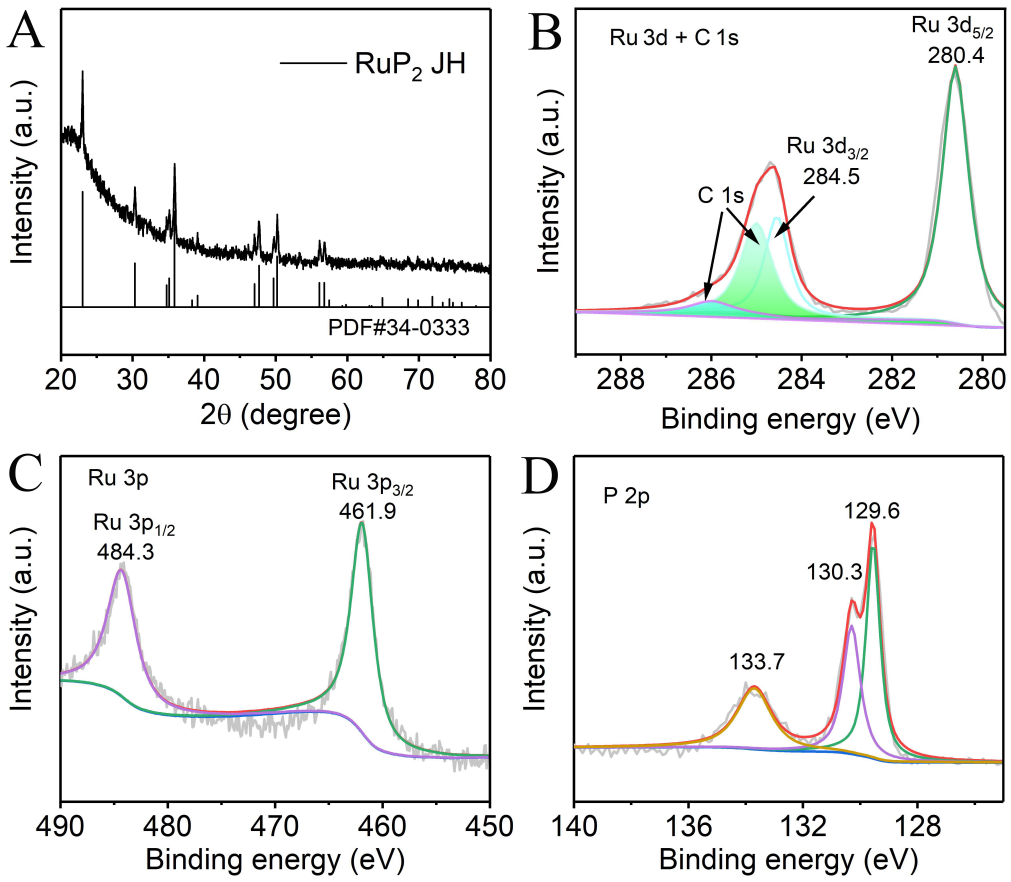

Figure 2. (A) The XRD pattern for RuP_2 JH. XPS spectra in the (B) Ru 3d and C 1s; (C) Ru 3p and (D) P 2p regions for RuP_2 JH. XRD: X-ray powder diffraction; XPS: X-ray photoelectron spectroscopic.

during the subsequent HER process. Therefore, the formation of the RuP_2 phase by Joule heating is unequivocally confirmed through comprehensive characterizations using TEM, XRD, and XPS techniques. Notably, a slight surface passivation effect is observed in RuP_2 JH.

The HER activity of the RuP_2 JH was examined in 0.5 M H_2SO_4 electrolytes, with all potentials calibrated using an RHE as the reference scale. Before conducting the HER tests, the RuP_2 JH material was activated by performing a series of linear sweep voltammetry (LSV) scans ranging from 0 V to -0.5 V *vs.* SCE. In order to facilitate comparison, we also assessed the HER catalytic activities of bulk RuP_2 (bulk RuP_2, obtained by a traditional method as reported in our previous work)[30], and commercial Pt/C under identical conditions. Typically, Figure 3A illustrates the HER polarization curves over RuP_2 JH, bulk RuP_2 and commercial Pt/C. The polarization curves of all HER measurements were *iR*-corrected, with the internal resistance determined through EIS analysis [Supplementary Figure 6]. The RuP_2 JH shows remarkable HER catalytic activities, as anticipated, with an onset potential close to 0 mV. It is worth noting that Pt/C, RuP_2 JH and bulk RuP_2 electrodes were tested three times for each sample. Specifically, as illustrated in Figure 3B, in 0.5 M H_2SO_4 solutions, the overpotentials needed for RuP_2 JH to achieve cathodic current densities of 10 mA cm^{-2}, 50 mA cm^{-2}, and 100 mA cm^{-2} are 22±1.5 mV, 67±3 mV and 95±2.5 mV, respectively. Notably, such outstanding HER performance of RuP_2 JH is comparable to the state-of-the-art commercial Pt/C catalysts (20 mV, 48 mV, and 92 mV). However, the bulk RuP_2 synthesized by conventional pyrolysis techniques exhibits a relatively modest HER activity of 130 mV at 10 mA cm^{-2}. Furthermore, the intrinsic

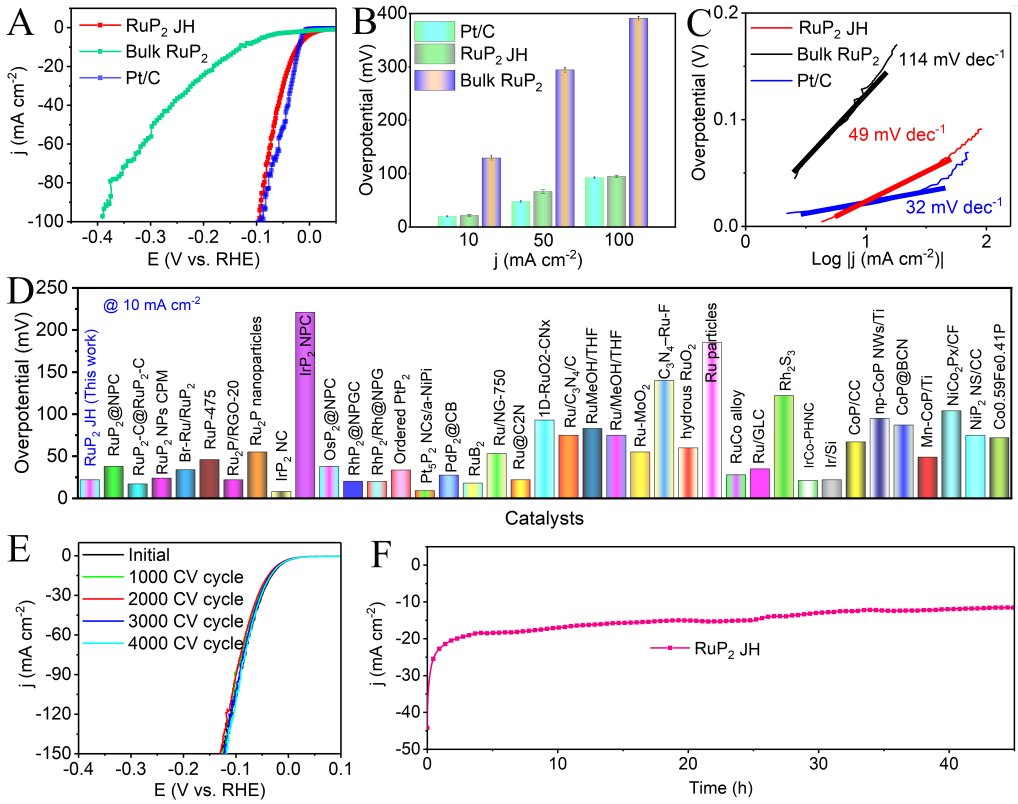

Figure 3. (A and C) Polarization curves and corresponding Tafel plots of commercial Pt/C, RuP_2 JH and bulk RuP_2 in 0.5 M H_2SO_4 solution; (B) Overpotentials at j = 10, 50 and 100 mA cm^{-2} for Pt/C, RuP_2 JH and bulk RuP_2, the error bars represent the standard deviations of three samples, with three measurements conducted for each sample; (D) Overpotentials comparison of RuP_2 JH at j = 10 mA cm^{-2} with recently reported HER electrocatalysts; (E) Polarization curves were recorded before and after 1000, 2000, 3000 and 4000 CV potential cycles for RuP_2 JH; (F) Chronoamperometric test for RuP_2 JH in 0.5 M sulfuric acid electrolyte at constant potential for 45 h (without *iR* correction). HER: Hydrogen evolution reaction.

performance of RuP_2 JH is further demonstrated by normalizing the HER activity with respect to the mass of Ru [Supplementary Figure 7]. More importantly, the catalytic activity of RuP_2 JH surpasses that of recently reported Ru-based TMPs, including RuP_2NPC (38 mV@10 mA cm^{-2}, Tafel slope 38 mV dec^{-1})[15], RuP_2 double-walled nanotubes synthesized through anion/cation exchange reactions (46 mV@10 mA cm^{-2})[34], and pure RuP synthesized by 24 h thermal treatment (36 mV@10 mA cm^{-2}, Tafel slope 39.8 mV dec^{-1})[35]. Similarly, the Tafel slope obtained from the linear region of the Tafel plots for RuP_2 JH is 49 mV dec^{-1} [Figure 3C], representing a notable improvement compared to that observed for bulk RuP_2 (114 mV dec^{-1}). This observation suggests the superiority of Joule heating over conventional methods in preparing RuP_2. Furthermore, to the best of our knowledge, the remarkable performance of RuP_2 JH is favorably compared to that of most TMPs synthesized using traditional strategies and other PGM-based materials for HER reported in acidic electrolytes [Figure 3D and Supplementary Table 1].

The long-term stability of RuP_2 JH was investigated using cyclic voltammetry (CV). Figure 3E presents the polarization curves obtained before and after 1000, 2000, 3000 and 4000 CVs at 5 mV s^{-1}. As depicted in Figure 3E, negligible degradation was observed in the LSV curves of RuP_2 JH even after undergoing 4000 CV potential cycles. Furthermore, the long-term durability of the RuP_2 JH electrocatalyst is investigated through continuous electrolysis at a fixed overpotential of approximately 50 mV. As shown in Figure 3F, the current density of RuP_2 JH exhibits only minimal degradation under acidic conditions during a 45 h electrolysis period, thereby indicating the excellent durability of the as-synthesized RuP_2 JH.

Additionally, the XRD analysis of the fresh and post-HER RuP_2 JH materials [Supplementary Figure 8] confirms the similarity in their crystal structures, providing further evidence for the preservation of RuP_2 JH composition and its exceptional durability towards HER under acidic media. Therefore, these comprehensive analyses unequivocally establish RuP_2 JH as an excellent and enduring catalyst material for the HER.

The investigation into the FE of hydrogen evolution by the RuP_2 JH catalyst is further extended. Specifically, the water drainage strategy has been used to quantify the amount of the generated H_2. The presence of generated H_2 bubbles on the working electrode surface is easily discernible [Supplementary Figure 9]. In addition, Supplementary Video 1 captures the dynamic process of HER and subsequent accumulation of hydrogen gas. As illustrated in Supplementary Figure 10, upon collecting the evolved hydrogen at a specific time, the quantity closely corresponds to the theoretical value predicted by Faraday's law, indicating an FE exceeding 96% for RuP_2 JH [Supplementary Figure 11]. The results unequivocally demonstrate that RuP_2 JH serves as an exceptional and enduring catalyst for HER.

Furthermore, the HER performance of RuP_2 JH was investigated under both alkaline (1.0 M KOH) and neutral (0.1 M PBS) electrolytes. Specifically, as depicted in Figure 4A-C, RuP_2 JH exhibits remarkable catalytic performance in alkaline electrolytes with a low onset potential of approximately 0 mV and a modest Tafel slope of around 57 mV dec^{-1}. Moreover, the RuP_2 JH exhibits overpotentials of 22 mV and 92 mV in alkaline media to achieve current densities of 10 mA cm^{-2} and 50 mA cm^{-2}, respectively. Notably, the HER catalytic activity provided by RuP_2 JH surpasses that of commercial Pt/C even at a current density exceeding 25 mA cm^{-2}. Importantly, the exceptional HER activity of RuP_2 JH surpasses that of the majority of recently reported PGM-based TMPs in alkaline solutions [Figure 4D and Supplementary Table 2]. Similarly, as shown in Figure 4E-G, RuP_2 JH exhibits exceptional HER activity with an overpotential of approximately 65 mV at j = 2 mA cm^{-2} and a low Tafel slope of 86 mV dec^{-1} under 0.1 M PBS solution. Additionally, the chronopotentiometric analysis presented in Supplementary Figure 12 demonstrates that the RuP_2 JH catalyst exhibits good stability in HER for over 20 h under alkaline and neutral solutions at a current density of 10 mA cm^{-2}. Importantly, the superior HER activity of RuP_2 JH surpasses that of the majority of recently reported materials in neutral solutions [Supplementary Figure 13 and Supplementary Table 3]. These findings underscore the outstanding HER performance of RuP_2 JH over a wide pH range.

Based on the aforementioned analytical findings, the high HER performance of RuP_2 JH can be explained as follows. On the one hand, the ultrafast synthesis process of RuP_2 results in the formation of relatively small nanoparticles, which in turn enhances the electrochemically active surface area. On the other hand, the improved catalytic performance of RuP_2 JH may originate from the grain boundaries, which facilitate the formation of a high density of defects. These defects create a unique coordination environment around the atoms near the grain boundaries, leading to lattice strain effects that effectively modulate the electronic structure of the active site[36,37]. More importantly, the presence of grain boundaries not only contributes to the high catalytic activity for HER, but also improves the stability of the catalyst[38].

CONCLUSIONS

In summary, a rapid Joule heating process has been developed for the ultrafast synthesis of RuP_2 nanomaterials within nine seconds. Extensive physical characterizations have revealed that the RuP_2 JH nanomaterials possess abundant grain-boundary-rich structures, with an average nanoparticle size of approximately 40 nm. Experimental data suggest that RuP_2 JH, rich in grain boundaries, exhibits low overpotentials of 22 mV, 22 mV and 270 mV at j = 10 mA cm^{-2} under acid, alkaline, and neutral electrolytes, respectively. This exceptional HER activity is comparable to that of the most extensively reported TMPs

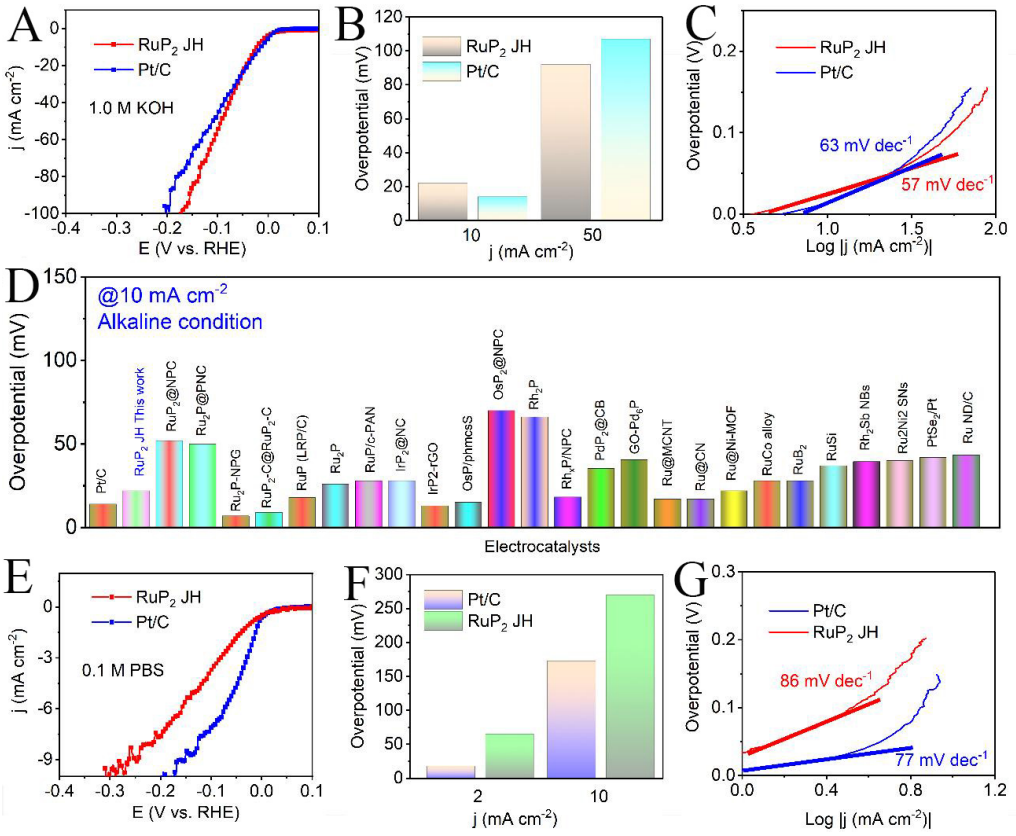

Figure 4. (A and E) LSV curves and (C and G) corresponding Tafel slopes for commercial Pt/C and RuP_2 JH in (A and C) alkaline and (E and G) neutral solutions; (B and F) Overpotentials at j = 2, 10 and 50 mA cm^{-2} for Pt/C and RuP_2 JH in (B) alkaline and (F) neutral solutions; (D) Overpotentials comparison of RuP_2 JH at j = 10 mA cm^{-2} with recently fabricated HER electrocatalysts in alkaline media. HER: Hydrogen evolution reaction; LSV: linear sweep voltammetry.

based on PGMs, which have traditionally been fabricated using solid-state or solution-phase strategies. Therefore, the Joule heating synthesis approach for RuP_2 at the seconds level holds significant promise for advancing the development of a range of TMP-based electrocatalysts in energy-related applications.

DECLARATIONS

Authors' contributions

Made substantial contributions to the conception and design of the study and performed data analysis and interpretation: Liu, T.; Chen, C.; Pu, Z.; Chen, Z.

Performed data acquisition and provided administrative, technical, and material support: Liu, T.; Chen, C.; Pu, Z.; Zhang, X.; Huang, Q.; Al-Enizi, A. M.; Nafady, A.; Sun, S.; Zhang, G.

Availability of data and materials

The data that support the findings of this study are available from the corresponding authors upon reasonable request.

Financial support and sponsorship

This work was supported by the Fonds de Recherche du Québec-Nature et Technologies (FRQNT), the National Natural Science Foundation of China (Grant No. 22402030), the Fujian Province Young and Middle-Aged Teacher Education Research Project (JZ230009). Al-Enizi, A. M and Pu, Z. extend their

appreciation to the Researchers Supporting Project number (RSP2025R55), King Saud University, Riyadh, Saudi Arabia for the funding support.

Conflicts of interest

All authors declared that there are no conflicts of interest.

Ethical approval and consent to participate

Not applicable.

Consent for publication

Not applicable.

Copyright

REFERENCES

1. Turner, J. A. Sustainable hydrogen production. *Science* **2004**, *305*, 972-4. DOI PubMed
2. Zhao, Y.; Niu, Z.; Zhao, J.; Xue, L.; Fu, X.; Long, J. Recent advancements in photoelectrochemical water splitting for hydrogen production. *Electrochem. Energy. Rev.* **2023**, *6*, 14. DOI
3. Pomerantseva, E.; Gogotsi, Y. Two-dimensional heterostructures for energy storage. *Nat. Energy.* **2017**, *2*, 17089. DOI
4. Ma, W.; Zhang, X.; Li, W.; et al. Advanced Pt-based electrocatalysts for the hydrogen evolution reaction in alkaline medium. *Nanoscale* **2023**, *15*, 11759-76. DOI
5. Li, Z.; Ge, R.; Su, J.; Chen, L. Recent progress in low Pt content electrocatalysts for hydrogen evolution reaction. *Adv. Mater. Inter.* **2020**, *7*, 2000396. DOI
6. Amano, F.; Tsushiro, K. Proton exchange membrane photoelectrochemical cell for water splitting under vapor feeding. *Energy. Mater.* **2024**, *4*, 400006. DOI
7. Huang, L.; Zaman, S.; Tian, X.; Wang, Z.; Fang, W.; Xia, B. Y. Advanced platinum-based oxygen reduction electrocatalysts for fuel cells. *Acc. Chem. Res.* **2021**, *54*, 311-22. DOI
8. Feng, J.; Li, J.; Zhang, H.; et al. Accelerating redox kinetics by ZIF-67 derived amorphous cobalt phosphide electrocatalyst for high-performance lithium-sulfur batteries. *Energy. Mater.* **2023**, *3*, 300001. DOI
9. Hu, C.; Hu, Y.; Zhang, B.; et al. Advanced catalyst design strategies and in-situ characterization techniques for enhancing electrocatalytic activity and stability of oxygen evolution reaction. *Electrochem. Energy. Rev.* **2024**, *7*, 19. DOI
10. Pu, Z.; Liu, T.; Amiinu, I. S.; et al. Transition-metal phosphides: activity origin, energy-related electrocatalysis applications, and synthetic strategies. *Adv. Funct. Mater.* **2020**, *30*, 2004009. DOI
11. Shi, Y.; Li, M.; Yu, Y.; Zhang, B. Recent advances in nanostructured transition metal phosphides: synthesis and energy-related applications. *Energy. Environ. Sci.* **2020**, *13*, 4564-82. DOI
12. Yu, S.; Cai, W.; Chen, L.; Song, L.; Song, Y. Recent advances of metal phosphides for Li-S chemistry. *J. Energy. Chem.* **2021**, *55*, 533-48. DOI
13. Chen, Z.; Zeng, X.; Li, X.; Lv, Z.; Li, J.; Zhang, Y. Strong metal phosphide-phosphate support interaction for enhanced non□noble metal catalysis. *Adv. Mater.* **2022**, *34*, 2106724. DOI
14. Pu, Z.; Liu, T.; Zhao, W.; et al. Versatile route to fabricate precious-metal phosphide electrocatalyst for acid-stable hydrogen oxidation and evolution reactions. *ACS. Appl. Mater. Interfaces.* **2020**, *12*, 11737-44. DOI
15. Pu, Z.; Amiinu, I. S.; Kou, Z.; Li, W.; Mu, S. RuP_2-based catalysts with platinum-like activity and higher durability for the hydrogen evolution reaction at all pH values. *Angew. Chem. Int. Ed.* **2017**, *56*, 11559-64. DOI PubMed
16. Ishikawa, H.; Yamaguchi, S.; Mizugaki, T.; Mitsudome, T. Highly active and sulfur-tolerant ruthenium phosphide catalyst for efficient reductive amination of carbonyl compounds. *ACS. Catal.* **2024**, *14*, 4501-9. DOI
17. Huang, C.; Xu, H.; Shuai, T.; Zhan, Q.; Zhang, Z.; Li, G. A review of modulation strategies for improving catalytic performance of transition metal phosphides for oxygen evolution reaction. *Appl. Catal. B. Environ.* **2023**, *325*, 122313. DOI
18. Wu, M.; Dong, F.; Yang, Y.; et al. Emerging atomically precise metal nanoclusters and ultrasmall nanoparticles for efficient electrochemical energy catalysis: synthesis strategies and surface/interface engineering. *Electrochem. Energy. Rev.* **2024**, *7*, 217. DOI
19. Yue, L.; Liang, J.; Wu, Z.; et al. Progress and perspective of metal phosphide/carbon heterostructure anodes for rechargeable ion batteries. *J. Mater. Chem. A.* **2021**, *9*, 11879-907. DOI
20. Xu, R.; Du, L.; Adekoya, D.; et al. Well-defined nanostructures for electrochemical energy conversion and storage. *Adv. Energy. Mater.* **2021**, *11*, 2001537. DOI
21. Kibsgaard, J.; Jaramillo, T. F. Molybdenum phosphosulfide: an active, acid-stable, earth-abundant catalyst for the hydrogen evolution

reaction. *Angew. Chem. Int. Ed.* **2014**, *53*, 14433-7. DOI PubMed

22. Xing, Z.; Liu, Q.; Asiri, A. M.; Sun, X. Closely interconnected network of molybdenum phosphide nanoparticles: a highly efficient electrocatalyst for generating hydrogen from water. *Adv. Mater.* **2014**, *26*, 5702-7. DOI
23. Li, C.; Wang, Z.; Liu, M.; et al. Ultrafast self-heating synthesis of robust heterogeneous nanocarbides for high current density hydrogen evolution reaction. *Nat. Commun.* **2022**, *13*, 3338. DOI PubMed PMC
24. Liu, W.; Yang, J.; Zhao, Y.; et al. Laser-ironing induced capping layer on Co-ZIF-L promoting in situ surface modification to high-spin oxide-carbon hybrids on the "real catalyst" for high OER activity and stability. *Adv. Mater.* **2024**, *36*, 2310106. DOI
25. Cui, M.; Yang, C.; Hwang, S.; et al. Rapid atomic ordering transformation toward intermetallic nanoparticles. *Nano. Lett.* **2022**, *22*, 255-62. DOI
26. Kim, Y. T.; Lee, J.; Lee, J. Electricity-driven reactors that promote thermochemical catalytic reactions via joule and induction heating. *Chem. Eng. J.* **2023**, *470*, 144333. DOI
27. Lv, X.; Tian, W.; Yuan, Z. Recent advances in high-efficiency electrocatalytic water splitting systems. *Electrochem. Energy. Rev.* **2023**, *6*, 23. DOI
28. Pu, Z.; Zhao, J.; Amiinu, I. S.; et al. A universal synthesis strategy for P-rich noble metal diphosphide-based electrocatalysts for the hydrogen evolution reaction. *Energy. Environ. Sci.* **2019**, *12*, 952-7. DOI
29. Du, H.; Du, Z.; Wang, T.; et al. Unlocking interfacial electron transfer of ruthenium phosphides by homologous core-shell design toward efficient hydrogen evolution and oxidation. *Adv. Mater.* **2022**, *34*, 2204624. DOI
30. Chen, D.; Pu, Z.; Lu, R.; et al. Ultralow Ru loading transition metal phosphides as high-efficient bifunctional electrocatalyst for a solar-to-hydrogen generation system. *Adv. Energy. Mater.* **2020**, *10*, 2000814. DOI
31. Liu, T.; Wang, J.; Zhong, C.; et al. Benchmarking three ruthenium phosphide phases for electrocatalysis of the hydrogen evolution reaction: experimental and theoretical insights. *Chem. Eur. J.* **2019**, *25*, 7826-30. DOI
32. Chang, Q.; Ma, J.; Zhu, Y.; et al. Controllable synthesis of ruthenium phosphides (RuP and RuP_2) for pH-universal hydrogen evolution reaction. *ACS. Sustainable. Chem. Eng.* **2018**, *6*, 6388-94. DOI
33. Jin, Y.; Fan, X.; Cheng, W.; Zhou, Y.; Xiao, L.; Luo, W. The role of phosphorus on alkaline hydrogen oxidation electrocatalysis for ruthenium phosphides. *Angew. Chem.* **2024**, *136*, e202406888. DOI
34. Hong, Y.; Cho, S. C.; Kim, S.; et al. Double-walled tubular heusler-type platinum-ruthenium phosphide as all-pH hydrogen evolution reaction catalyst outperforming platinum and ruthenium. *Adv. Energy. Mater.* **2024**, *14*, 2304269. DOI
35. Galyamin, D.; Torrero, J.; Elliott, J. D.; et al. Insights into the high activity of ruthenium phosphide for the production of hydrogen in proton exchange membrane water electrolyzers. *Adv. Energy. Sustain. Res.* **2023**, *4*, 2300059. DOI
36. Hu, C.; Yue, K.; Han, J.; et al. Misoriented high-entropy iridium ruthenium oxide for acidic water splitting. *Sci. Adv.* **2023**, *9*, eadf9144. DOI PubMed PMC
37. He, W.; Tan, X.; Guo, Y.; Xiao, Y.; Cui, H.; Wang, C. Grain-boundary-rich RuO_2 porous nanosheet for efficient and stable acidic water oxidation. *Angew. Chem. Int. Ed.* **2024**, *63*, e202405798. DOI
38. Geng, X.; Vega-Paredes, M.; Wang, Z.; et al. Grain boundary engineering for efficient and durable electrocatalysis. *Nat. Commun.* **2024**, *15*, 8534. DOI PubMed PMC